Iron-nickel metal foams modified by phosphides as robust catalysts for a hydrogen evolution reaction

Iron-nickel metal foams modified by phosphides as robust catalysts for a hydrogen evolution reaction

A. Gubóová[a], R. Oriňaková[a,b*], M. Strečková[c], M. Paračková[a], O. Petruš[c], B. Plešingerová[d], M. Mičušík[e]

[a] Institute of Chemistry, Faculty of Science, P. J. Šafárik University, Moyzesova 11, 040 01 Košice, Slovakia

[b] Centre of Polymer Systems, University Institute, Tomas Bata University in Zlín, Třída Tomáše Bati 5678, 76001 Zlín, Czech Republic

[c] Institute of Materials Research, Slovak Academy of Sciences, Watsonova 47, 040 01 Košice, Slovakia

[d] Faculty of Materials, Metallurgy and Recycling, Technical University, Letná 9, 042 00 Košice, Slovakia

[e] Polymer Institute, Slovak Academy of Sciences, Dúbravská cesta 9, 845 41 Bratislava 45, Slovakia

1 Introduction

The pressing need for clean and renewable energy sources stems from far-reaching environmental issues caused by rapid fossil fuel depletion and the use of non-renewable energy sources. Pollution of the environment caused by excessive consumption of energy is an inevitable issue that needs to be promptly addressed by the development of clean and suitable energy sources [1, 2]. One of the most compelling alternatives is hydrogen due to its high energy density and non-polluting properties [3]. Hydrogen is a great pure chemical fuel alternative for providing stable and renewable energy [4].

Electrochemical water splitting is a promising approach to hydrogen production due to its environmental and sustainability benefits [2]. The main advantage of this process is that no carbon dioxide emissions are released [5]. In addition, if solar, wind or generally renewable energy is used as the energy source, the result is a completely green, clean and highly ecological process, and thus pure, environmentally friendly hydrogen [6].

The hydrogen evolution reaction (HER) is a cathodic reaction in electrochemical water splitting. Decomposition of water in its simplest form uses an electric current passing through

two electrodes (cathode and anode) to split water into hydrogen and oxygen. Basically, it is conversion of electricity into chemical energy in the form of hydrogen, with oxygen as a useful by-product. The theoretical voltage requirement for the overall water splitting reaction is only 1.23V, although a higher voltage is required to overcome reaction barrier [3].

Numerous attempts have been made to fabricate efficient electrode material that would act as a superior electrocatalyst for HER [4, 5]. The ideal HER catalyst with optimal properties is one that is efficient, stable and affordable at the same time. To date, the most efficient catalysts for HER are platinum group metals (including Pt, Ru, Rh, Ir and Pd), known as noble metals, due to their high conductivity and electrocatalytic properties. However, the high price and scarcity of these metals motivate the scientific community to search for competitive low-cost alternatives [2]. In order to make the technology of water-splitting to obtain hydrogen more affordable, it is necessary to find inexpensive and efficient catalysts that would act as a substitute for precious metals [7].

The numerous advantages of electrochemical water splitting are still being overshadowed by the low efficiency of the process [8]. A way to overcome this shortcoming is to optimize electrode materials for electrolyzers and fuel cells. The goal is to keep costs low while reducing overpotentials and increasing stability and activity. The crucial characteristic of the electrode material is its morphology. A large specific surface area has a critical effect, and high porosity provides accessibility and economical use of the material, which together boost the electrochemical activity towards hydrogen evolution [9].

Transition metals (TM), such as iron, nickel, cobalt or copper, are becoming satisfactory cost-efficient alternatives to precious metals [10]. They are Earth-abundant, relatively cheap and exhibit rather high catalytic activity for water splitting. Nickel exhibits exceptional catalytic activity in alkaline solutions [5, 11]. Different types of TM catalyst, such as sulfides, phosphides or nitrides, have been investigated with varying success in meeting the electrocatalytic needs of HER [12, 13]. Despite the great importance for catalytic reactions and numerous efforts, the development of affordable and easy synthesis of a transition metal catalyst for HER is still a challenging task [3].

In electrocatalysis, the use of porous electrodes is widespread mainly to reduce overpotential of the reaction by increasing the real surface area [7]. From the point of view of the electrocatalytic hydrogen evolution, catalysts based on matrices doped with nanoparticles of a transition metal (e.g., Co, Ni, Fe, Cu) have been investigated in detail [14, 15, 16]. The increased

electrocatalytic performance of such materials is associated with embedded nanoparticles of metals and a metal compound (phosphide, nitride etc.), which can facilitate the transport of electrons through the matrix. Another suitable option is metal foams, which can serve as a substrate and can be further modified according to specific needs.

Foams in general represent a unique construction material, characterized by high porosity and thus high surface area resulting in a structure with low resistance to the flow of fluids [1].

The use of metal foams is widespread due to their exceptional properties, including a high stiffness-to-weight ratio, porous structure and compression energy absorption. Nickel-base alloys have a special position among metal foams. Their nature makes them perfect candidates for catalytic substrates, but also supercapacitors or heat exchangers and filters [17]. Immense efforts are being made to improve some of the mechanical and microstructural properties of nickel-based foams to further improve their suitability for commercial use. Despite extensive research [9, 14, 18], the performance of nickel catalyst for HER needs to be further improved to be considered a viable alternative to Pt catalysts.

Another option for the preparation of porous metal catalysts is the place-holder technique. This technique is based on sintering a mixture of a metal component and a placeholder component that removes the placeholder element and creates pores in the material structure. Hao Li et al. [19] sintered nickel oxalate (NiC_2O_4) with sodium chloride (NaCl) with a necessary reduction step. Their results showed NaCl to be an efficient separator preventing direct contact between the nickel particles, thus providing a porous structure. Another approach to obtain a porous metal material is leaching. Usually, two or more metal powders are mixed together and compressed under specific pressure. Then the leaching process is carried out in either a strong acid or a strong base solution. For example, nickel powder can be used with zinc or aluminum, which are then leached out overnight in sodium hydroxide solution [7].

Metal foam catalysts can also be prepared by the 3D printing method, but this process has significant disadvantages, such as design inaccuracies, limited build size or materials, since the choice of raw materials is short. Porous metal foam can also be prepared by the slurry (metal powder or a metal compound and solvent, often also containing a dissolved polymer) coating of a polymer template. This is called the replication method and uses an open cell structure as a template, which is coated with metal powder slurry and then removed by sintering to obtain a metallic material with a porous structure [20].

Nickel and its composites and alloys are widely studied for application in hydrogen evolution due to high corrosion resistance in alkaline solutions and exceptional stability among the transition metals (far exceeding that of iron or cobalt) [18].

A logical step in the development of a sustainable catalyst is to combine inexpensive metals with adequate catalytic activity instead of using noble metals such as platinum [21]. Iron phosphates are intensively studied due to their advantages in large-scale applications, namely high activity toward HER, high conductivity and the abundance of iron, which reduces costs and increases the possibility of commercialization [22, 23].

Feng Ye et al. analyzed the effect of different Ni/Co ratios on the catalytic activity of porous heterostructured NiCoP/NF catalysts. The highest catalytic activity was recorded for Ni:Co= 1:3 ratio, with overpotential value of 99 mV (at 10 $mA.cm^{-2}$) and a Tafel slope of 65.44 $mV.dec^{-1}$ [24]. Gao et al. synthesized a NiCoP-CoP/Ni/NF catalyst via direct growth on nickel foam, which showed phenomenal catalytic activity in alkaline media with overpotential required to reach 10 $mA.cm^{-2}$ being only 49 mV [25]. Zhou et al. used hydrothermal method followed by phosphorization to obtain FeCoNi-P/NF nanosheet arrays with stability over 60 hours in alkaline media. Increased active sites growth as well as improved electron transport resulted in impressive catalytic properties, such as a Tafel slope of only 61.2 $mV.dec^{-1}$ and an overpotential of 266 mV to achieve a current density of 50 $mA.cm^{-2}$ [26]. Cong Li et al. investigated the possibility of preparing iron and cobalt phosphates using the colloidal chemical method. The best performance was observed for the $Fe_{0.72}Co_{0.42}PO_4$/Ni foam catalyst, which achieved excellent results, such as an overpotential needed to reach current density of 10 $mA.cm^{-2}$ of 77 mV, which is comparable to platinum [27].

Bandal et al. studied growth of FeCoO on nickel foam. The catalyst attained a current density of 10 $mA.cm^{-2}$ at an overpotential of 244 mV and 205 mV for OER and HER, respectively. When applied in electrolyzer, FeCoO-NF achieved a current density of 10 $mA.cm^{-2}$ at an overpotential of 1.62 V. The outstanding catalytic performance is attributed to the hierarchical structure, which promotes the electrolyte transfer, the perfect electrolyte-catalyst contact and the inclusion of iron in the cobalt oxide structure [28].

The replication method, based on the impregnation of polyurethane (PUR) foams with a suspension of metal powder and gelatin and subsequent sintering, is a promising, inexpensive and simple method of preparing metal foams. In this work, three different metal foams (Ni, FeNi and Fe) were prepared by the replication method and then modified with sodium

hypophosphite monohydrate using temperature-programmed reduction (TPR) in H_2 atmosphere. It was found that NiP and FeP, which were formed on the surface of metal foams during phosphorization, showed electrocatalytic activity and facilitated HER. The electrocatalytic activity and stability of all prepared foam materials were evaluated using linear sweep voltammetry (LSV) and chronopotentiometry. The morphological analyses were performed regarding the porosity determined by Hg porosimetry.

2 Experimental

2.1 Chemicals

Iron powder (spherical <10 μm, 99.9+% (metals basis), 99.5%, Alfa Aesar), nickel powder (<50 μm, 99.7% trace metals basis, MW 58.69 $g.mol^{-1}$, Sigma Aldrich) and an equimolar mixture (1:1) of both powders were used as base materials for the preparation of metallic foams, as well as gelatin (granular, for analysis, Acros Ogranics). Sodium phosphate monobasic dihydrate ($NaH_2PO_2.H_2O$; >99%, for molecular biology, Biotech) was used in the subsequent phosphorization treatment as a source of phosphorus. All chemicals were used without further purification.

2.2 Samples preparation

One of the most important factors affecting the structural and mechanical properties of porous metal foams is the process of removal of the porous organic substrate (e.g., the PUR foam). Most polymeric substrate removal methods use a two-step thermal treatment, where in the first step the substrate is removed (usually by burning in an air, nitrogen or argon atmosphere) and in the second step the obtained metal foam is annealed. This step is performed in a reductive atmosphere to prevent oxidation and to achieve the desired structure [29].

Metal porous foams were prepared by a replication method as shown in Figure 1. To prepare the suspension, 1 g of gelatin was dissolved in distilled water at 60 °C and used as polymeric binder to ensure uniform distribution of the metal slurry on the PUR foam. The gelatin and polyurethane foam were then removed by a sintering process. Then, iron powder or nickel powder or a mixture of both was added to the gelatin solution. The PUR foam was cut into rectangular pieces ($1\times1\times2$ cm^3) and subsequently impregnated with a suspension of metal powder and gelatin. Excess suspension was removed to prevent the clogging of the pores. To obtain the desired porous structure, the prepared samples were dried at 200 °C for 5 minutes and then sintered in a tube furnace at 450 °C for 2 hours under a nitrogen atmosphere to remove

the PUR foam and gelatin. In the second step, the metal foams were annealed for 1 hour in a reduction atmosphere (90% nitrogen, 10% hydrogen) at 1120 °C for Fe samples and at 1200 °C for Ni and FeNi samples. The preparation conditions are summarized in Table 1 in the Supporting Information (SI).

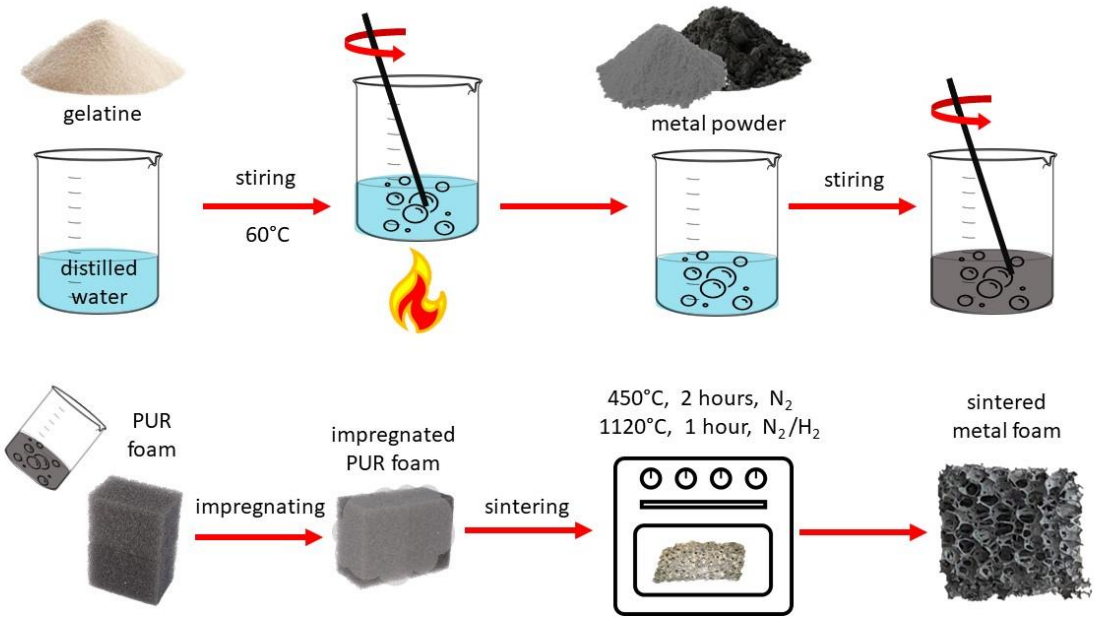

Figure 1 Schematic preparation of metal foam samples

The phosphorization process of the as-prepared metal foams was realized by temperature-programmed reduction in a H_2 atmosphere [30]. First, the metal foams were cleaned, and the surface layers of oxides were removed by successive immersion in acetone, a solution of 1 M HCl for 10–15 minutes, and simultaneously sonicated. Then, the metallic foams were dried at room temperature and placed on a ceramic boat. Another ceramic boat containing $NaH_2PO_2.H_2O$ powder was placed in the furnace in front of the boat with sample along the gas stream and heated to 300°C at a rate of 1°C/min. The samples were kept at this temperature for 2 hours and then cooled back to room temperature, rinsed with deionized water and dried at 60°C under vacuum. The final products were labeled as FeP, FeNiP and NiP.

2.3 Methods

The morphology and elemental composition of the metal foams were visualized using a scanning electron microscope (JSM-7000F, JEOL, Japan) equipped with an EDX detector (Oxford Instruments, England).

The size and distribution of the pores were determined using a mercury porosimeter (Quantachrome PoreMaster 33).

The phase composition of the samples was done via XRD analysis with a CuKα radiation source.

The XPS analysis was applied to confirm the formation of phosphides using a Thermo Scientific Nexsa G2 Surface Analysis System (Thermo Fisher Scientific, UK) equipped with a microfocused, monochromatic Al Kα X-ray source (1486.68 eV). The spectra for the survey were acquired in constant analyzer energy mode with a pass energy of 200 eV. Narrow spectral regions were collected using a pass energy of 50 eV. Charge compensation was achieved with an Ar flood gun system. Thermo Scientific Avantage software, version 6.6.0 (Thermo Fisher Scientific), was used for digital acquisition and data processing. The surface compositions (in atomic %) were determined by considering the integrated peak areas of the detected atoms and the respective sensitivity factor.

Electrochemical characterization was performed in a three electrode electrochemical cell connected to a PGSTAT302N potentiostat (Metrohm Autolab, Netherlands). LSV measurements were performed in a 1M KOH solution at a scan rate of 1 $mV.s^{-1}$ in the potential range from 300 mV to -1800 mV for HER and in the range from 0 mV to 1300 mV for OER. A saturated calomel electrode (SCE) and a large area (~ $1cm^2$) platinum electrode were used as the reference and the counter electrode, respectively. Metal foams were used as working electrodes, while part of the sample with a volume of 1 cm^3 was immersed in the electrolyte solution. All potentials were referenced to the reversible hydrogen electrode (RHE) using equation (1). Current densities were calculated using the electroactive surface area determined by electrochemical double layer capacitance. All polarization curves were measured without iR compensation.

$$E_{RHE} = E_{SCE} + 0.059.pH + 0.242 \quad (1)$$

Electrochemical impedance spectra were recorded in a frequency range from 100 kHz to 10 mHz with an AC voltage amplitude of 5 mV at an overpotential of -0.5 V vs RHE for HER and +1.6 V vs RHE for OER. Additionally, the most active samples were studied as bifunctional catalysts and directly employed as the cathode and anode to study their behavior in a simulated electrolyzer-like set up. Bifunctional measurements were carried out in an alkaline media in the potential range from 0 mV to 2000 mV with a scan rate $1mV.s^{-1}$. The overall stability of the

samples was evaluated by means of a long-term stability test, where the change in potential over time was recorded at a constant current of 10 $mA.cm^{-2}$ for 22 hours in an alkaline medium.

3 Results and discussion:

Although iron might not be the most preferred transition metal for the hydrogen evolution reaction due to its corroding nature, its performance when mixed with nickel provides excellent results while maintaining low cost and good availability. Stability and corrosion issues can be easily overcome by using alkaline media instead of an unsuitable acidic environment. The reason for avoiding other transition metals in this work, such as cobalt, which is otherwise widely used in HER catalysis, is its inclusion on a list of critical raw materials (for EU) [31].

3.1 Surface morphology and composition

The morphologies of the as-prepared metal foams were investigated by scanning electron microscopy. All the metal foam samples show a rather uniform structure with explicit open pores, even though there are noticeable filled spots where the coating suspension merged and filled in the pore gap.

The distribution and size of the pores revealed different features depending on the metals used for the metal foam preparation. All micropore sizes as well as wall thickness obtained from image analysis are summarized in Table 1, whereas additional size range distribution with standard deviations can be found in Figure 2 in the SI. The application of pure Fe led to an enlargement of the open macropores, which reached a size of approximately 860 ± 240 µm, which corresponds to the pore size of the polyurethane foam used as a matrix. The wall thickness was around 115 ± 86 µm.

The structure of the individual samples is clearly different, with a visibly finer porosity in the nickel matrix filled by smaller pores (in the range from approximately 362 µm) in comparison with pure Fe foam (747 µm)- Fig. 2. The surface of the foams is highly structured, which can be attributed to the spherical shape of the metal powder particles used as base materials.

Table 1 Micropore size and wall thickness of individual samples

Sample	*Pore size [µm]*	*Wall thickness [µm]*
Fe	747 ± 94	81 ± 11
FeP	733 ± 55	72 ± 6
FeNi	369 ± 23	111 ± 33

FeNiP	438 ± 61	156 ± 29
Ni	362 ± 128	229 ± 79
NiP	440 ± 126	217 ± 104

The chemical composition of the bare metal foams and the mass ratio of iron and nickel determined by EDX analysis are summarized in Table 2 in the SI. The EDX analysis confirmed the equimolar composition of the mixed samples and the uniform distribution of metals in the foams.

A similar trend in pore size and wall thickness was observed after phosphorization of the metallic foams (Fig. 3). The largest pores were detected in the case of phosphorized Fe foam and the smallest in the case of phosphorized Ni foam. The opposite trend occurred in the case of wall thickness, which increased in the order: Fe 81 μm < FeNi 111 μm < Ni 217 μm.

The mapping EDX analysis of phosphorized foams confirmed the presence of phosphorus (Fig. 3). FeP foam contained 81.3% iron and 7.8% phosphorus. The remaining 11.0% were detected as oxygen, either because of the formation of $FePO_x$ instead of FeP, or, more likely, due to oxidation of the metal on account of keeping the samples exposed to air. The same effect was visible for NiP foams, where the oxygen content was only 3.2%, with a nickel majority of 87.1% and the highest content of phosphorus among the samples at 9.7%. The combined FeNiP sample did not involve any oxygen, and the phosphorus content was the same as for the iron sample. The iron to nickel content was almost the same (47.1% iron and 45.1% nickel).

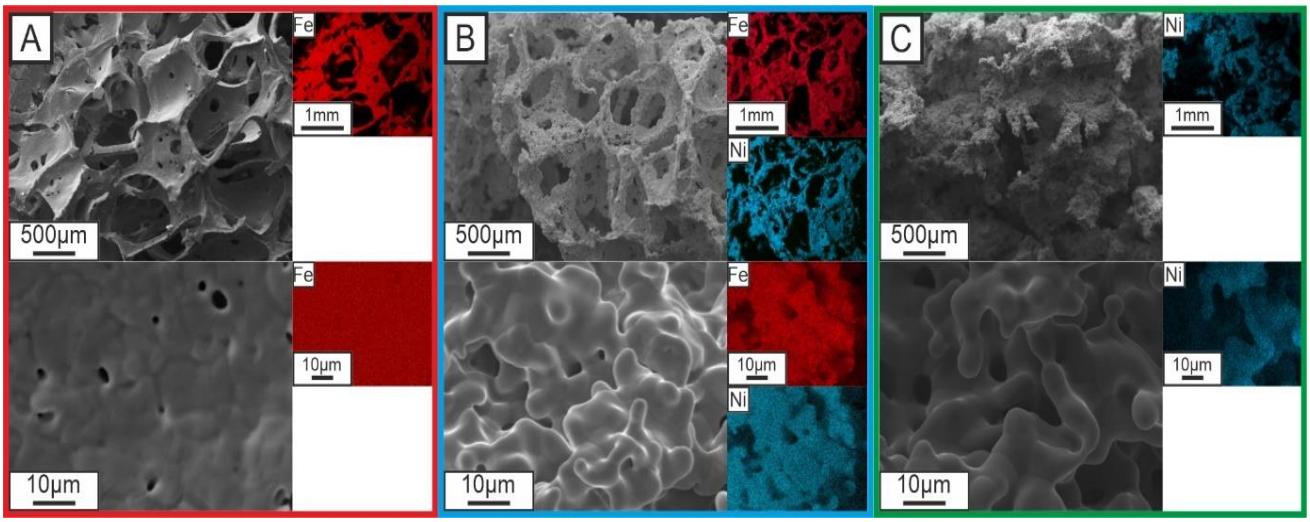

Figure 2 SEM images and EDX analysis of Fe, FeNi and Ni foams

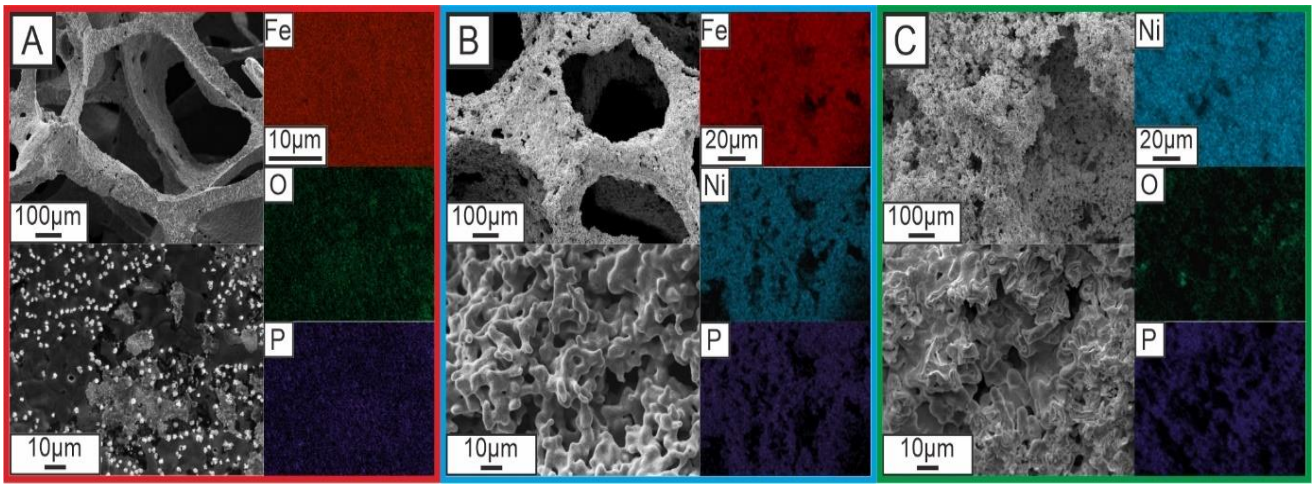

Figure 3 SEM images and EDX analysis of phosphorized FeP, FeNiP and NiP foams

The concept of mercury porosimetry lies in the pressure-dependent penetration of mercury into the pores of the studied samples [32]. The pore size distribution obtained using Hg porosimetry, together with normalised volume for the Fe, FeNi and Ni samples, is shown in Fig. 4.

The pore size values obtained by porosimetry are in agreement with the results obtained by analyzing the SEM images of the individual samples. The iron samples consist of a large number of large pores (around 1000 μm) as well as a large number of medium pores (between 10–100 μm) with very small pores being less represented (Fig. 4 (a)). For the FeNi samples (Fig. 4 (b)), most of the pores are in the size range from 1 to 10 μm, and as the pore size increases, so does their number. Some larger pores (>100 μm) are also represented. The Ni sample (Fig. 4 (c)) shows the most Gaussian distribution, with most pores in the size range from 0.1 to 1 μm. Table 4 summarizes the porosity, surface area, average pore diameter and pore volume of pure metal foams obtained using the mercury porosimetry method. The surface area of the Ni foam sample is almost 400 times larger than that of the Fe foam with the absence of smaller micropores. However, the overall porosity of the Ni foam is about half the porosity compared to the Fe sample with large pores (greater than 1 micrometer). The pore analysis was not performed for the phosphorized samples because the phosphorus content was not significant enough to enable difference to be detected.

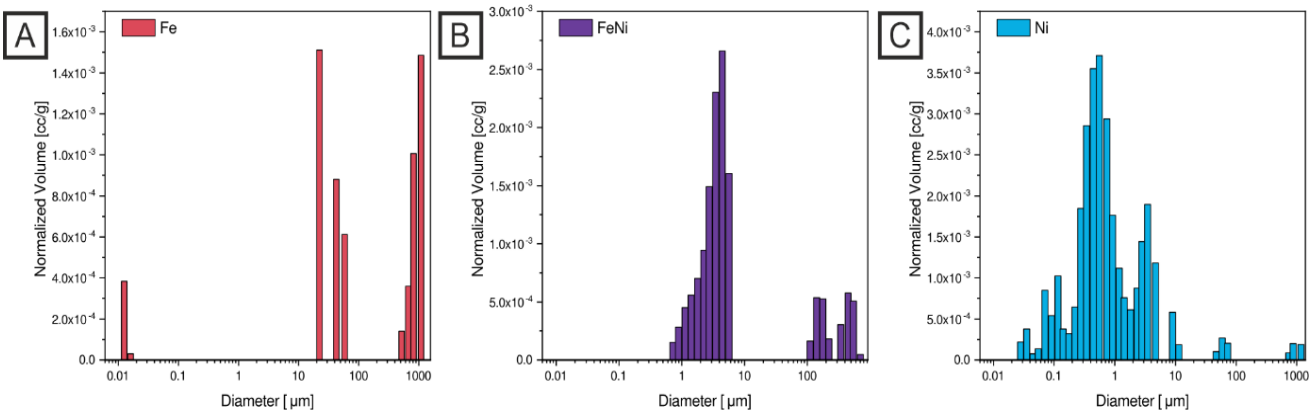

Figure 4 Pore size distribution of pure metal foams (a) Fe, (b) FeNi, (c) Ni obtained by mercury porosimetry

Table 2 Porosity, surface area and average diameter obtained by mercury porosimetry analysis

Sample	*Porosity [%]*	*Average diameter [µm]*	*Surface [$cm^2.g^{-1}$]*
Fe	69	122	4
FeNi	47	56	169
Ni	31	31	1560

The crystallographic structure of the prepared foam materials was determined using X-ray diffraction analysis (XRD). The diffraction peaks at 44.7°, 65.1° and 82.4° can be indexed to the (110), (200) and (211) planes of Fe (JCPDS No. 06-0696) with body-centered cubic structure [33]. The diffraction peaks of FeNi and Ni were at 43.7°, 50.9° and 74.9° corresponding to the (111), (200) and (220) planes, which match with the face-centered cubic structure of Ni (JCPDS no 00-004-0850) and bulk FeNi alloy. [34]. The small amount of P in the phosphorized foams caused the XRD analysis to be unable to detect the presence of the created phosphides. Therefore, to characterize the surface composition and to confirm the formation of phosphides on the surface of the metal foams, X-ray photoelectron spectroscopy (XPS) measurements were performed. XPS survey spectra show the presence of Fe2p, Ni2p, P2p, C1s, O1s and some impurities as Na1s, K2p, Sn3d, Si2p and F1s (Figure 6, Table XPS). The oxygen content is attributed to the surface oxidation due to exposure of the samples in air and some surface contamination by adventitious carbon (C-O) and some other impurities coming from the sample handling or from the rather complex wet chemistry preparation method. Fe $2p_{3/2}$ peak at 709-712 eV represents the Fe^{2+} (ca 709 eV) and Fe^{3+} (ca 711eV) in a chemical bond with oxygen or as phosphates. $Fe2p_{3/2}$ signal was used for chemical structure

evaluation but is overlapped with Ni auger peaks (*Ni LM4* and *Ni LM5*, Figure 6b), so the quantification of iron was done with $Fe2p_{1/2}$ in order to have more precise iron evaluation. Fe $2p_{3/2}$ peak at 706.7 eV represents either metallic iron or the Fe-P bond in the case of phosphorized samples. P $2p_{3/2}$ signal at ca 129 eV confirms the presence of phosphides on the surface (Figure 6d). The P 2p spectra also include a peak at 133 eV, which represents the P-O bond indicating the oxidation of the surface and the presence of phosphates (PO_4) [35]. In the Ni $2p_{3/2}$ spectrum Ni^{2+} species (either NiO – at ca 853.4 eV or $Ni(OH)_2/Ni_3(PO_4)_2$ – at ca 855.7 eV) with typical satellite features for $Ni(OH)_2/Ni_3(PO_4)_2$ at 861-866 eV are visible. Ni metal signal at ca 852.6 eV is clearly visible only in the case of Ni sample (Figure 6c), at this position should be also metal-P bonds in the case of phosphorized samples [36]. In the phosphorized samples of NiP and NiFeP the presence of phosphides is confirmed only by relatively low signal of P2p at ca 129 eV (0.4 at.% of metal-P bonds, Table XPS) presumably due to substantial surface oxidation of the samples [37]. NiP sample shows also some traces of iron (0.5 at.%), which has relatively high chemical shift ($Fe2p_{3/2}$ at ca 714 eV), which together with the presence of F1s signal at ca 688 eV (0.3 at. %) indicate some contamination with Fe-F species. In summary, these results confirm the successful synthesis of a phosphide surface layer on iron and nickel metal foam catalysts, but the surface is in some cases almost fully oxidized.

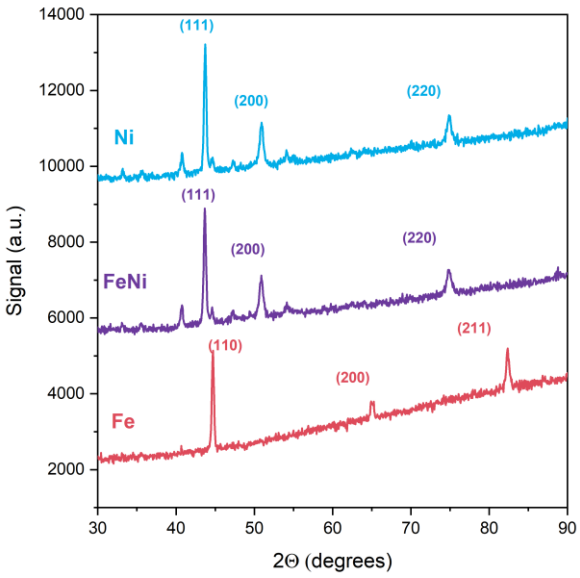

Figure 5 The X-ray diffraction patterns of the nickel, nickel-iron and iron samples

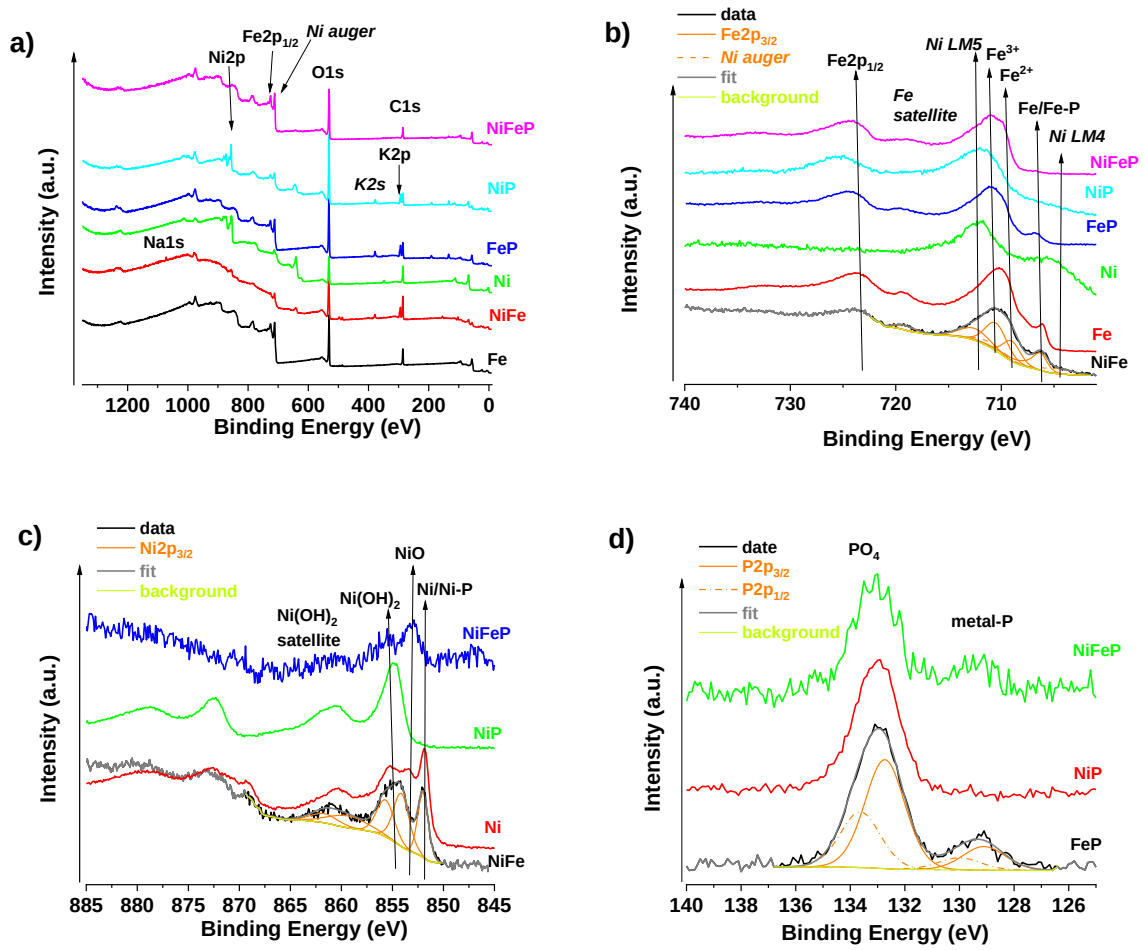

Figure 6 XPS of a) survey spectra of all samples, b) Fe2p region, c) Ni2p region and d) P2p region

Table XPS. Apparent surface chemical composition as determined by XPS.

sample	Surface chemical composition (at.%)					
	C1s C-C/C-O*	O1s	$Fe2p_{1/2}$ Fe-P/Fe^{2+}/Fe^{3+}	Ni2p NiP/Ni^{2+}	P2p P/P-O	Ca2p/K2p/Sn3d/F1s/Na1s/N1s/Si2p
Fe	34.9 26.2/8.7	48.3	16.7 3.2/2.4/11.0	—	—	—/—/0.2/—/—/—/—/—
FeNi	40.0 33.5/6.5	44.4	1.8 0.3/0.3/1.2	1.9 0.5/1.4	—	—/5.3/0.2/—/1.0/0.3/5.1
Ni	45.8 37.9/7.9	35.4	—	17.1 3.6/13.5	—	1.4/0.1/0.1/—/—
FeP	24.0 17.2/6.8	53.1	9.5 1.4/2.4/5.7	—	7.8 1.5/6.3	—/5.6/—/—/—/—/—

NiP	17.1	60.7	0.5	11.9	5.0	—/4.5/—/0.3/—/—
	9.8/7.3		—/—/0.5	—/11.9	0.4/4.6	/—
FeNiP	28.5	53.1	16.6	0.4	1.3	—/—/—/—/—/—/
	22.5/6.0		0.7/2.6/13.3	0.5/1.4	0.4/0.9	—

* includes all oxygen bonds with carbon as C-O, C=O, OC=O

3.2 Electrochemical performance

3.2.1 Hydrogen evolution reaction

Electrochemical activity towards hydrogen evolution was evaluated using polarization curves. The LSV curves for all the prepared metal foams (bare and phosphorized) are presented in Fig. 6). In general, the phosphorized samples showed higher catalytic activity than the unmodified ones. As expected, due to the different active surface area of the individual foams, nickel showed better catalytic performance than iron with the overpotential to achieve a current density of 10 $mA.cm^{-2}$ being -155 mV for nickel and -220 mV for iron. This indicates that the very large pores of the iron foam revealed by mercury porosimetry and visualized by SEM images may not be desirable due to the smaller surface area available for reaction. In contrast, medium- to small-sized pores enlarge the accessible surface, which results in improved catalytic activity for nickel foams. The polarization curve for FeNi foam lies between the curves for Ni and Fe, indicating that the catalytic activity of the mixed foams is worse than that of Ni, but better than that of Fe samples, with an overpotential value of -187 mV. All measured values of the HER process are summarized in Tab. 3. The activity of FeP is significantly higher compared to Fe foam, with an overpotential value of -85 mV. The catalytic performance of FeNiP is significantly higher, too, with a value of only -43 mV. For the phosphorized nickel sample the overpotential to achieve a current density -10 $mA.cm^{-2}$ is -63 mV, which is roughly half the value for the unphosphorized sample. The considerably lower values for phosphorized samples indicate a significant increase in activity, which makes this treatment highly desirable for achieving better catalytic performance.

For further investigation of the catalytic activity of the foams, the Tafel plots obtained from the polarization curves (Fig. 8 B)) were used. Smaller slope values indicate higher reaction rates. The theoretical values of the Tafel slope around 30 $mV.dec^{-1}$, 40 $mV.dec^{-1}$ and 120 $mV.dec^{-1}$ are calculated for the Tafel, Heyrovsky and Volmer steps, respectively [38]. The determined

values of the Tafel slopes of 103.6 mV.dec^{-1}, 92.0 mV.dec^{-1} and 70.5 mV.dec^{-1} for Fe, FeNi and Ni foams, respectively, indicate that the Volmer step was the rate-determining step (RDS) for the bare metal samples. Similar values of the Tafel slopes of 105.7 mV.dec^{-1} and 73.7 mV.dec^{-1} were obtained for the FeP and FeNiP samples, indicating the same RDS; however, the NiP foam achieved a Tafel slope value of 47.1 mV.dec^{-1}, suggesting Heyrovsky RDS and thus the Volmer-Tafel mechanism.

Table 3 Values of overpotentials at current densities of 10mA.cm^{-2}, 20 mA.cm^{-2} and 100mA.cm^{-2}; exchange current densities and Tafel slopes for all samples

Sample	η_{10} *[mV]*	η_{20} *[mV]*	η_{100} *[mV]*	j_0 *[mA.cm^{-2}]*	*b [mV.dec^{-1}]*
Fe	-220	-380	-638	4.40	103.6
FeP	-85	-178	-416	3.96	105.7
FeNi	-187	-270	-467	3.57	92.0
FeNiP	-43	-99	-309	5.53	73.7
Ni	-155	-204	-391	4.45	70.5
NiP	-63	-125	-393	4.61	47.1

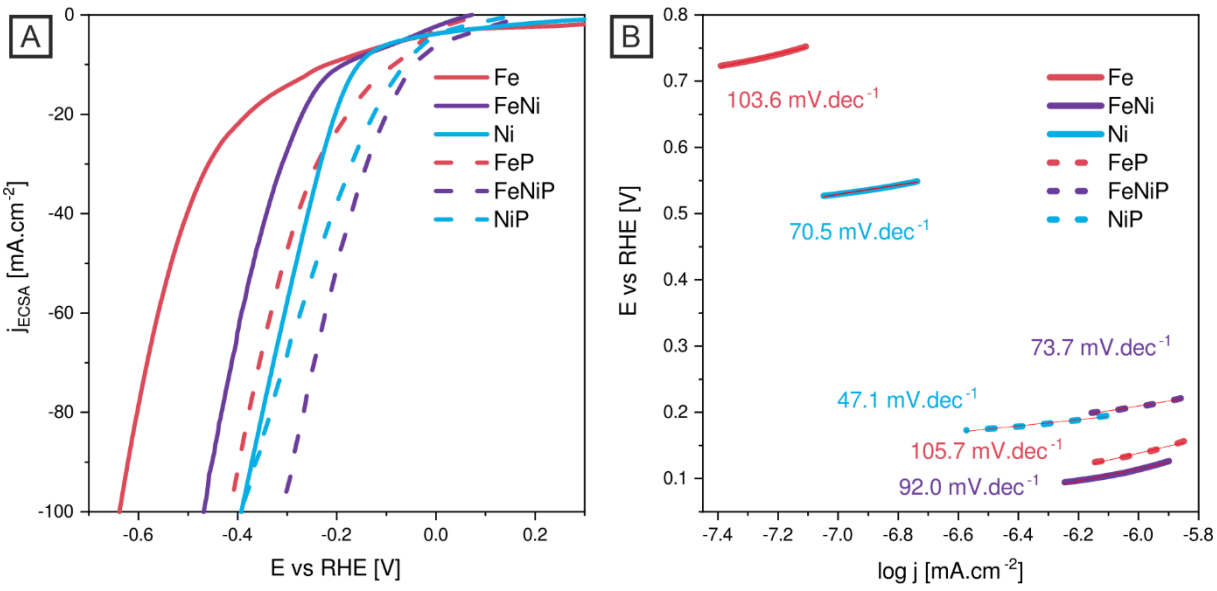

Figure 7 A) HER Polarization curves for pure metal foams and phosphorized metal foams in alkaline media (1M KOH) B) Tafel slopes of pure and phosphorized iron/nickel metal foams with respective b-constant values

As is evident from the mercury porosimetry measurements, the iron samples have a smaller surface area. On the other hand, the nickel samples are comprised of smaller pores which contribute to much greater surface area, thus providing more active sites for the reaction to proceed. The measured double-layer capacitances presented in Fig. 7 also confirm these results. The iron samples exhibited much lower double-layer capacitance than the other samples, with NiP having the highest value, as expected, for the best performing catalyst. The C_{dl} value is closely related to the active surface area according to equation (1) described in the SI; therefore, the foam samples with the highest values of C_{dl} (like Ni and NiP or NiFe) provide the largest active surface area for electrochemical process. High capacitance values also indicate higher catalytic activity, since more active catalysts are inclined to have a higher C_{dl} value [39] [40].

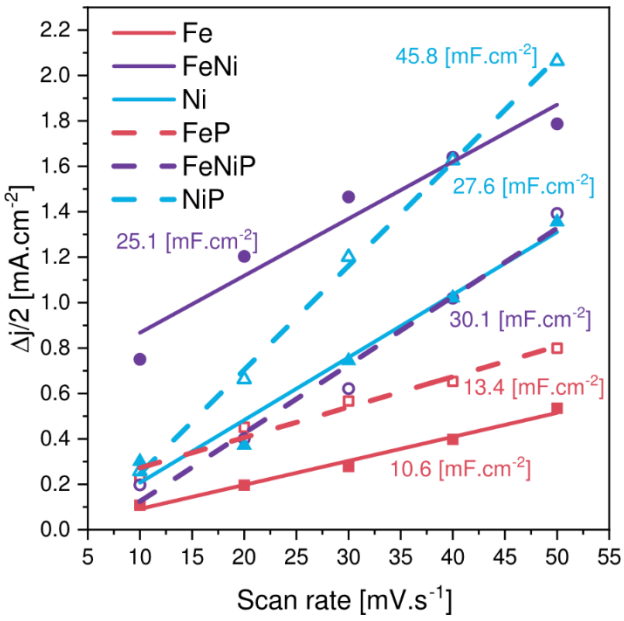

Figure 8 Measured capacitive currents plotted as a function of the scan rate

Electrochemical impedance spectroscopy was used to provide insight into the charge transfer between the electrode and the electrolyte and the conductivity properties of the metal foams. The measured EIS spectra are shown in Fig. 8. The Nyquist plots were fitted using an equivalent circuit consisting of Rs, Rp and CPE. The single semicircle in the high frequency area reveals the charge transfer resistance between the electrolyte and the electrode [41]. Rs refers to the resistance of the solution. The exceptional activity is caused by the large electrochemically active surface area (ESCA) and small mass transfer resistances [25]. The semicircles are slightly asymmetric; the curves have more moderate slope in the high frequency area, and in the low

frequency area the slope is steeper. This is more evident for the Fe and FeP samples. The EIS results are consistent with the electrocatalytic performance. An equivalent circuit used to fit all measured spectra is shown in Figure 9 A. The resistance values presented in Table 4 show that the Rp of NiP (0.587 Ω) is lowest among all the samples, while fitting the results for Ni and FeNiP show similar values of 0.756 Ω and 0.786 Ω, respectively. The highest Rp value was recorded for pure Fe (2.07 Ω), which is in accordance with the results of other electrochemical evaluations and indicates slower electron transport for pure iron samples.

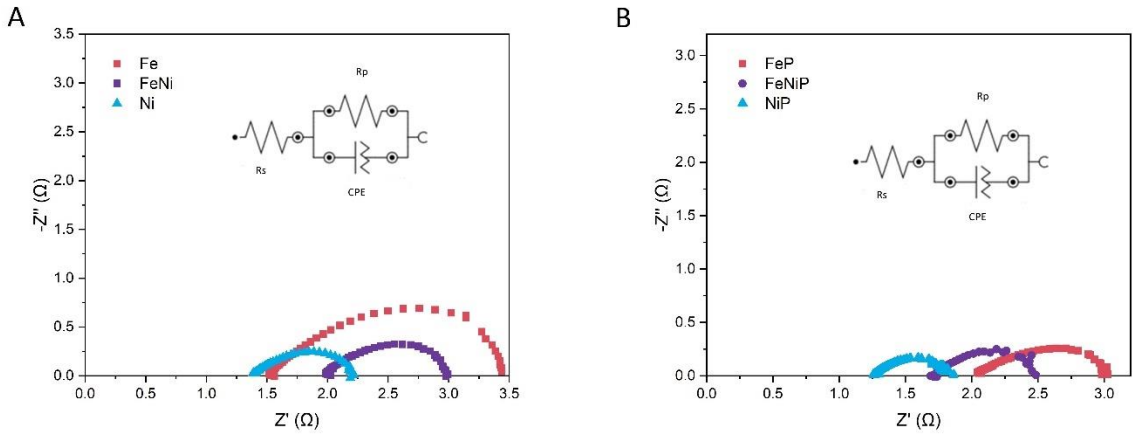

Figure 9 Nyquist plots of the electrical impedance measurements for HER for M/MP foams at -500 mV vs. RHE in 1M KOH

Table 4 Resistance values for M/MP foams obtained by fitting HER Nyquist plots with an equivalent circuit

Sample	Rp [Ω]	Rs [Ω]
Fe	2.07	1.53
FeNi	1.02	2.00
Ni	0.756	1.40
FeP	1.02	2.05
FeNiP	0.786	1.72
NiP	0.587	1.26

3.2.2 Oxygen evolution reaction

The catalytic performance of the prepared foam samples towards the oxygen evolution reaction was investigated by obtaining polarization curves (Fig. 9 A) under similar conditions as with the HER measurements. The values of overpotentials at current densities of 10 $mA.cm^{-2}$, 20 $mA.cm^{-2}$ and 100 $mA.cm^{-2}$, exchange current densities and Tafel slopes for the OER process

are summarized in Table 5. The NiP sample showed excellent electrocatalytic activity, with an overpotential of 261 mV to achieve a current density of 10 $mA.cm^{-1}$. The Ni sample exhibited an even lower overpotential of 203 mV, but this was due to a significant oxidation peak, common in OER for nickel catalysts in an alkaline environment. The activity of all the foam samples in OER showed the same trend as that in HER, with activity increasing and overpotentials required to reach a current density of 10 $mA.cm^{-2}$ decreasing in the order FeNiP < FeNi < FeP < Fe, with values of 313 mV, 335 mV, 364 mV and 466 mV, respectively. This trend was the same even for a current density of 20 $mA.cm^{-2}$, but it changed with increasing current, and at a current density of 100 $mA.cm^{-2}$ the FeNiP showed a significantly lower overpotential (503 mV) than NiP (590 mV). These results suggest that the mixed FeNiP catalyst might be more suitable for commercial application.

Table 5 Values of overpotentials at current densities of 10$mA.cm^{-2}$, 20 $mA.cm^{-2}$ and 100$mA.cm^{-2}$, exchange current densities and Tafel slopes for all samples

Sample	η_{10} *[mV]*	η_{20} *[mV]*	η_{100} *[mV]*	j_0 *[$mA.cm^{-2}$]*	*b [$mV.dec^{-1}$]*
Fe	466	505	611	*0.616*	*145.2*
FeP	364	431	649	*0.234*	*101.7*
FeNi	335	363	523	*0.141*	*82.4*
FeNiP	313	338	503	*3.02*	*78.5*
Ni	203*	329	578	*0.813*	*50.1*
NiP	261	304	590	*0.479*	*44.5*

*-oxidation peak

The Tafel slope values for NiP and Ni (Fig. 9 B), as low as 44.5 $mV.dec^{-1}$ and 50.1 $mV.dec^{-1}$, respectively, imply fast charge transfer kinetics. The Tafel slope of the FeNiP foam sample, with a value of 78.5 $mV.dec^{-1}$, indicates slower kinetics, despite the highest value of the exchange current density (3.02 $mA.cm^{-2}$), which confirms the assumption of the suitability of the mixed sample for use in energy conversion devices.

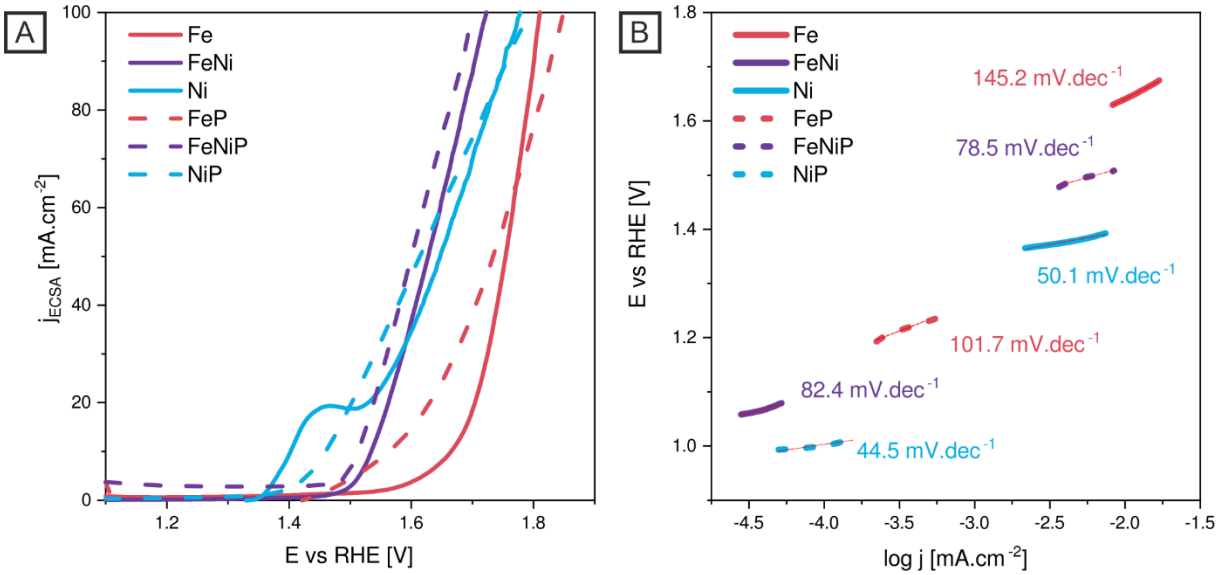

Figure 10 A) OER Polarization curves for pure metal foams and phosphorized metal foams in alkaline media (1M KOH) B) Tafel slopes of pure and phosphorized iron/nickel metal foams with respective b-constant values

The measured EIS spectra for OER are shown in Fig. 10. Nyquist plots were fitted using the same equivalent circuit as for HER, consisting of Rs, Rp and CPE. The resistance values are provided in Table 6 and the fitting results display the lowest Rp value of 1.18 Ω for the NiP sample. A very similar value (1.22 Ω) was recorded for FeNiP, signifying the fastest electron transport among the studied catalysts. The spectra show a single semicircle, similar to the EIS measured for HER; however, the semicircles for FeNi and Ni as well as FeNiP and NiP foams are significantly smaller than the semicircles for Fe/FeP foams. This is associated with much higher charge transfer resistance for the iron samples. The semicircles are more symmetrical, especially for phosphorized samples.

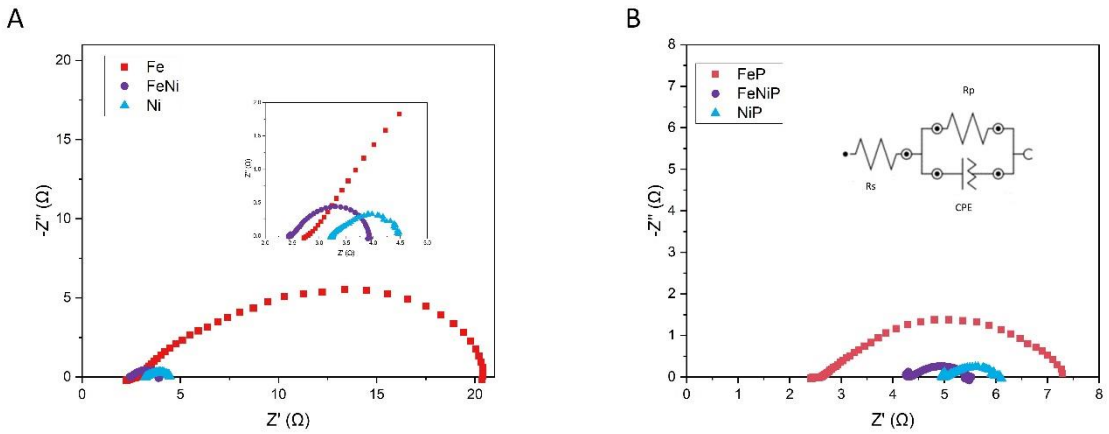

Figure 11 Nyquist plots of the electroimpedance measurements for OER for M/MP foams at 600 mV vs. RHE in 1M KOH

Table 6 Resistance values for M/MP foams obtained by fitting OER Nyquist plots with equivalent circuit

Sample	Rp [Ω]	Rs [Ω]
Fe	1.86	3.32
FeNi	1.50	2.46
Ni	1.35	3.23
FeP	1.29	2.50
FeNiP	1.22	2.29
NiP	1.18	1.96

3.2.3 Bifunctional performance

To evaluate the bifunctional performance, the two most active foam catalysts (NiP and FeNiP) were tested in an alkaline water splitting electrolyzer-like setup using the same foam as both cathode and anode (FeNiP-FeNiP and NiP-NiP). The measured polarization curves without iR compensation are depicted in Fig.11 A). The water decomposition potential, that is, the overpotential to attain a current density of 10 $mA.cm^{-2}$, was 1.66 V and 1.61V for FeNiP and NiP, respectively. Such a low potential indicates excellent activity of the prepared catalytic materials for water decomposition in an alkaline environment.

The stability of the most active catalysts was also evaluated, as it is one of the most important characteristics of catalysts and their possible commercial use in electrolyzers. The stability of the foam samples was assessed using the chronopotentiometric method, and the obtained E-t curves are shown in Fig. 11 B). Both samples showed good stability for at least 22 hours. The SEM images obtained after the long-term stability test reveal very small morphological changes on both cathode and anode surfaces, probably caused by vigorous bubbling during hydrogen and oxygen evolution. Additional SEM images acquired after stability test are provided in the SI (Fig. 4, Fig. 5).

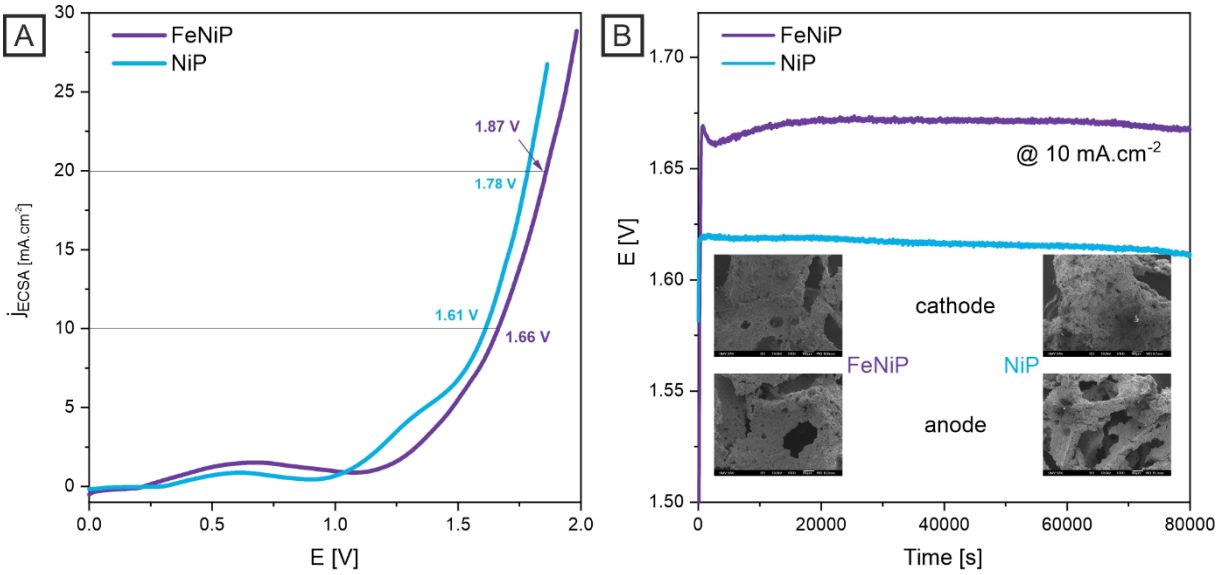

Figure 12 a) Bifunctional measurement of FeNiP and NiP catalysts in 1M KOH to determine activity for overall water splitting b) Stability test at 10 mA.cm^{-2} for 22 hours

To better compare the obtained results with the literature,

Table 7 summarizes parameters such as the values of the overpotential required to achieve a current density of -10 mA.cm^{-2}, as well as the values of the Tafel slopes for similar catalysts based on iron and/or nickel. The bare nickel foams prepared in this work exhibited better catalytic performance than the nickel sample (nickel deposited on nickel foam) and commercial nickel foam with values of the overpotential needed to achieve a current density of 10 mA.cm^{-2} of -155 mV, -250 mV and -271 mV, respectively. The phosphorus-containing catalysts showed lower overpotentials than similar catalysts without phosphorus, indicating that the incorporation of P into the samples is an effective method to increase the activity, and thus the phosphorization of the foams is a suitable method to improve their electrocatalytic properties. The porous Ni and FeNi catalysts also showed relatively low values of Tafel slopes compared to other samples. The presented results show that the prepared metal foams exhibited comparable or even higher HER performance than published catalysts based on iron and nickel.

Table 7 Comparison of results

Catalyst	*electrolyte*	*η_{10} [mV]*	*b [mV/dec]*	*reference*
FeNiP	KOH	-43	73.7	This work

NiP	KOH	-63	47.1	This work
Ni foam	KOH	-271	147	[5]
Nickel pure*	KOH	-250	86	[5]
NiFeP/SG	KOH	-115	47	[42]
FeP-Fe@NC	H_2SO_4	-97	88	[43]
Ni-Fe foam (5%Fe)	H_2SO_4	~ -250**	100.45	[44]

*Nickel deposited on nickel foam

**Extrapolated from graph

4 Conclusion

The aim of this work was to prepare effective platinum-free catalysts containing more abundant and affordable transition metals, such as iron and nickel. A relatively simple replication method based on the impregnation of the polymer matrix, which was subsequently removed by the sintering process, was used to fabricate metallic foams. The prepared metal foams were subsequently modified by a phosphorization process, which resulted in the formation of foam samples with a layer of phosphides on the surface (FeP, NiP and FeNiP). Significant differences in the porosity of unmodified foam samples (Fe, FeNi and Ni) were detected by Hg porosimetry. The highest catalytic activity in an alkaline environment was observed for FeNiP and NiP catalysts, which showed values of the overpotentials necessary to reach a current density of 10 $mA.cm^{-2}$ of only -43 mV and -63 mV for HER and 313 mV and 261 mV for OER, thus enabling bifunctional use. Both catalysts also exhibited outstanding activity in the simulated electrolyzer assembly, while achieving a current density of 10 $mA.cm^{-2}$ at overpotentials of 1.66 V (FeNiP) and 1.61 V (NiP) and a current density of 20 $mA.cm^{-2}$ at overpotentials of 1.87 V (FeNiP) and 1.78V (NiP). They also demonstrated excellent stability for at least 22 hours.

Author Contributions

A. Gubóová: Investigation, Methodology, Data curation, Writing- original draft. **R. Oriňaková:** Funding acquisition, Writing- review and editing. **M. Strečková:** Funding acquisition, Writing- review and editing. **M. Paračková:** Investigation, Data curation **O.**

Petruš: Investigation, Data curation, Methodology. **B. Plešingerová:** Investigation, Data curation. **M. Mičušík:** Investigation, Data curation.

Conflicts of interest

There are no conflicts to declare.

Acknowledgement

This work was supported by the Scientific Grant Agency of the Ministry of Education, Science, Research and Sport of the Slovak Republic (project VEGA 1/0095/21 and VEGA 2/0027/23), and the Slovak Research and Development Agency (project APVV-20-0299 and no. APVV-20-0576).

Data availability

The raw/processed data required to reproduce these findings are available on request from the authors.

References

[1] E.A. Moreira, M.D.M. Innocentini, J.R. Coury, "Permeability of ceramic foams to compressible and incompressible flow," *Journal of the European Ceramic Society,* vol. 24, no. 10-11, pp. 3209-3218, 2004.

[2] Sajjad Hussain, Dhanasekaran Vikraman, Linh Truong, Kamran Akbar, Iqra Rabani, Hyun-Seok Kim, Seung-Hyun Chun, Jongwan Jung,, "Facile and cost-effective growth of MoS2 on 3D porous graphene-coated Ni foam for robust and stable hydrogen evolution reaction,," *Journal of Alloys and Compounds,* vol. 788, pp. 267-276, 2019.

[3] Jianqing Zhou, Luo Yu, Qiancheng Zhou, Chuqiang Huang, Yuanlu Zhang, Bo Yu, Ying Yu,, "Ultrafast fabrication of porous transition metal foams for efficient electrocatalytic water splitting,," *Applied Catalysis B: Environmental,,* vol. 288, 2021.

[4] H. Fayaz, R. Saidur, N. Razali, F.S. Anuar, A.R. Saleman, M.R. Islam, "An overview of hydrogen as a vehicle fuel," *Renew Sustain Energy Rev,* vol. 16, pp. 5511-5528, 2012.

[5] N. Lotfi, T. Shahrabi Farahani, Y. Yaghoubinezhad, Gh. Barati Darband,, "Simulation and characterization of hydrogen evolution reaction on porous NiCu electrode using surface response methodology,," *International Journal of Hydrogen Energy,,* vol. 44, no. 26, pp. 13296-13309, 2019.

[6] K.I. Siwek, S. Eugénio, D.M.F. Santos, M.T. Silva, M.F. Montemor,, "3D nickel foams with controlled morphologies for hydrogen evolution reaction in highly alkaline media,," *International Journal of Hydrogen Energy,,* vol. 44, no. 3, pp. 1701-1709, 2019.

[7] C Hitz, A Lasia, "Experimental study and modeling of impedance of the her on porous Ni electrodes," *Journal of Electroanalytical Chemistry,* vol. 500, no. 1-2, pp. 213-222, 2001.

[8] A. Lasia, Handbook of fuel cells – fundamentals, technology and applications, vol. 2, vol. Chap. 4.6, Chichester: John Wiley & Sons, 2003.

[9] D.M.F. Santos, S. Eugénio, C.A.C. Sequeira, M.F. Montemor, "Transition metal foam electrocatalysts for hydrogen evolution reaction," *ECS Trans,* vol. 64, pp. 9-16, 2015.

[10] P. Du, R. Eisenberg, "Catalysts made of earth-abundant elements (Co, Ni, Fe) for water splitting: recent progress and future challenges," *energy Environ Sci,* vol. 5, pp. 6012-6021, 2012.

[11] I. Herraiz-Cardona, E. Ortega, J.G. Antón, V. Pérez-Herranz, "Assessment of the roughness factor effect and the intrinsic catalytic activity for hydrogen evolution reaction on Ni-based electrodeposits," *Int J Hydrogen energy,* vol. 36, pp. 9428-9438, 2011.

[12] C. Huang, L. Yu, W. Zhang, Q. Xiao, J. Zhou, Y. Zhang, P. An, J. Zhang, Y. Yu, "N-doped Ni-Mo based sulfides for high-efficiency and stable hydrogen evolution reaction," *Applied Catalysis B,* no. 119137, p. 276, 2020.

[13] L. Shang, Y. Zhao, X. Kong, R. Shi, G.I.N. Waterhouse, L. Wen, T. Zhang, "Underwater superaerophobic Ni nanoparticle-decorated nickel–molybdenum nitride nanowire arrays for hydrogen evolution in neutral media," *Nano Energy*, vol. 78, no. 105375, 2020.

[14] Y. Xiao, Y. Liu, Z. Tang, L. Wu, Y. Zeng, Y. Xu, et al., "Porous Ni-Cr-Fe alloys as cathode materials for hydrogen evolution reaction," *RSC Adv*, vol. 6, pp. 51096-51105, 2016.

[15] Lu, Xue Feng, Le Yu, and Xiong Wen Lou, "Highly crystalline Ni-doped FeP/carbon hollow nanorods as all-pH efficient and durable hydrogen evolving electrocatalysts," *Science advances*, vol. 5, no. 2, 2019.

[16] Xiang Peng, Abdul Mateen Qasim, Weihong Jin, Lei Wang, Liangsheng Hu, Yaping Miao, Wan Li, Yong Li, Zhitian Liu, Kaifu Huo, Kwok-yin Wong, Paul K. Chu, "Ni-doped amorphous iron phosphide nanoparticles on TiN nanowire arrays: An advanced alkaline hydrogen evolution electrocatalyst," *Nano Energy*, vol. 53, pp. 66-73, 2018.

[17] J. Xu, Y. Sun, M. Lu, L. Wang, J. Zhang, J. Qian, and X. Liu, "Metal oxide-based supercapacitors: progress and prospectives," *Chemical Energy Journal*, vol. 334, pp. 1466-1476, 2018.

[18] F. Safizadeh, E. Ghali, G. Houlachi, "Electrocatalysis developments for hydrogen evolution reaction in alkaline solutions – a review," *Int J Hydrogen Energy*, vol. 40, pp. 256-274, 2015.

[19] Hao Li, Rutie Liu, Jie Chen, Zhubo Wang, Xiang Xiong, "Preparation of nickel porous materials by sintering nickel oxalate and sodium chloride after blending and reduction," *Journal of Materials Research and Technology*, vol. 9, no. 3, pp. 3149-3157, 2020.

[20] A. Kennedy, "Porous metals and metal foams made from powders," *Powder Metallurgy*, vol. 2, pp. 31-46, 2012.

[21] Shengyu Ma, Jun Deng, Yaping Xu, Weiying Tao, Xiaoqi Wang, Zhiping Lin, Qinghua Zhang, Lin Gu, Wenwu Zhong, "Pollen-like self-supported FeIr alloy for improved hydrogen evolution reaction in acid electrolyte," *Journal of Energy Chemistry*, vol. 66, pp. 560-565, 2022.

[22] Xinglong Zhang, Yulin He, Bin Zhu, Xinming Wan, Shiyang Hua, Hui Tang, "A bottom-up method to construct Ru-doped FeP nanosheets on foam iron with ultra-high activity for hydrogen evolution reaction," *International Journal of Hydrogen Energy*, vol. 48, no. 12, pp. 4686-4693, 2023.

[23] Xin-Yu Zhang, Jing-Yi Xie, Yu Ma, Bin Dong, Chen-Guang Liu, Yong-Ming Chai, "An overview of the active sites in transition metal electrocatalysts and their practical activity for hydrogen evolution reaction," *Chemical Engineering Journal*, vol. 430, no. 3, p. 132312, 2022.

[24] Feng Ye, Yakun Yang, Peng Liu, Yuancheng Feng, Yanpeng Cao, Duanhao Cao, La Ta, Xiaofeng Ma, Chao Xu, "In-situ porous flake heterostructured NiCoP/Ni foam as electrocatalyst for hydrogen evolution reaction," *Electrochimica Acta*, vol. 423, p. 140578, 2022.

[25] Xingchen Gao, Kaixin Lu, Jianjun Chen, Jie Min, Deliang Zhu, Manlin Tan, "NiCoP–CoP heterostructural nanowires grown on hierarchical Ni foam as a novel electrocatalyst for efficient hydrogen evolution reaction," *International Journal of Hydrogen Energy*, vol. 46, no. 45, pp. 23205-23213, 2021.

[26] Chenmin Zhou, Jianshuai Mu, Yu-Feng Qi, Qian Wang, Xiao-Jun Zhao, En-Cui Yang, "Iron-substituted Co-Ni phosphides immobilized on Ni foam as efficient self-supported 3D hierarchical electrocatalysts for oxygen evolution reaction," *International Journal of Hydrogen Energy*, vol. 44, no. 16, pp. 8156-8165, 2019.

[27] Cong Li, Xuanhao Mei, Frank Leung-Yuk Lam, and Xijun Hu, "Amorphous Iron and Cobalt Based Phosphate Nanosheets Supported on Nickel Foam as Superior Catalysts for Hydrogen Evolution Reaction," *ACS Applied Energy Materials*, vol. 1, no. 12, pp. 6764-6768, 2018.

[28] Harshad A. Bandal, Amol R. Jadhav, Asif H. Tamboli, Hern Kim, "Bimetallic iron cobalt oxide self-supported on Ni-Foam: An efficient bifunctional electrocatalyst for oxygen and hydrogen evolution reaction," *Electrochimica Acta*, vol. 249, pp. 253-262, 2017.

[29] Faeze Barzegar, Akram Salehi, Ahmad Moloodi, "An Investigation of the Effect of Sintering Conditions on the Mechanical Behavior of Electroplated Nickel Foams," *Metallurgical and Materials Transactions B*, 2019.

[30] Jiale Xing, Zehua Zou, Kailu Guo, and Cailing Xu, "The effect of phosphating time on the electrocatalytic activity of nickel phosphide nanorod arrays grown on Ni foam," *Materials Research Society,* vol. 33, no. 5, pp. 556-567, 2017.

[31] Directorate-General for Internal Market, Industry, Entrepreneurship and SMEs, "Internal Market, Industry, Entrepreneurship and SMEs," an official website of the European Union, [Online]. Available: https://ec.europa.eu/growth/sectors/raw-materials/areas-specific-interest/critical-raw-materials_en. [Accessed 20th December 2021].

[32] Francisco Rodríguez-Reinoso, Antonio Sepúlveda-Escribano, "Chapter 9 - POROUS CARBONS IN ADSORPTION AND CATALYSIS," in *Handbook of Surfaces and Interfaces of Materials*, E. H. S. Nalwa, Ed., Academic Press, 2001, pp. 309-355.

[33] Yang, Pingan, Wenxian Ye, Haibo Ruan, Rui Li, Mengjie Shou, Yichen Yin, Xin Huang, Yuxin Zhang, Jiufei Luo, "Core–Shell Structured Silica-Coated Iron Nanowires Composites for Enhanced Electromagnetic Wave Absorption Properties," *International Journal of Molecular Sciences,* vol. 24, no. 10, p. 8620, 2023.

[34] Dijith, K. S., Aiswarya, R., Praveen, M., Pillai, S., & Surendran, K. P. , "Polyol derived Ni and NiFe alloys for effective shielding of electromagnetic interference," *Materials Chemistry Frontiers,* vol. 2, no. 10, pp. 1829-1841, 2018.

[35] Liu, D., Wu, C., Yan, M., & Wang, J. , "Correlating the microstructure, growth mechanism and magnetic properties of FeSiAl soft magnetic composites fabricated via HNO3 oxidation," *Acta Materialia,* vol. 146, pp. 294-303, 2018.

[36] Liu, P., Zhang, ZX., Jun, S.W. et al., "Controlled synthesis of nickel phosphide nanoparticles with pure-phase Ni2P and Ni12P5 for hydrogenation of nitrobenzene," *Reac Kinet Mech Cat,* vol. 126, pp. 453-461, 2019.

[37] Qingtao Wang, Minmin Hou, Yanna Huang et al, "One-pot synthesis of NiCoP/CNTs composites for lithium ion batteries and hydrogen evolution reaction," *Ionics,* vol. 26, pp. 1771-1778, 2020.

[38] Aisha Alobaid, Chunsheng Wang, Raymond A. Adomaitis, "Mechanism and Kinetics of HER and OER on NiFe LDH Films in an Alkaline Electrolyte," *Journal of The Electrochemical Society,* vol. 165, 2018.

[39] Lirong Huang, Yanping Hou, Zebin Yu, Zhenbo Peng, Li Wang, Jun Huang, Boge Zhang, Lun Qian, Leidan Wu, Zongchen Li, "Pt/Fe-NF electrode with high double-layer capacitance for efficient hydrogen evolution reaction in alkaline media," *International Journal of Hydrogen Energy,* vol. 42, no. 15, pp. 9458-9466, 2017.

[40] Sengeni Anantharaj, Hisashi Sugime, Suguru Noda, "Why shouldn't double-layer capacitance (Cdl) be always trusted to justify Faradaic electrocatalytic activity differences?," *Journal of Electroanalytical Chemistry,* vol. 903, p. 115842, 2021.

[41] Sining Yun, Yongwei Zhang, Lishan Zhang, Zhuolei Liu, Yingying Deng, "Ni and Fe nanoparticles, alloy and Ni/Fe-Nx coordination co-boost the catalytic activity of the carbon-based catalyst for triiodide reduction and hydrogen evolution reaction," *Journal of Colloid and Interface Science,* vol. 615, pp. 501-516, 2022.

[42] Rui-Qing Li, Bao-Lu Wang, Tian Gao, Ran Zhang, Chenyang Xu, Xiangfen Jiang, Jinjue Zeng, Yoshio Bando, Pengfei Hu, Yongle Li, Xue-Bin Wang, "Monolithic electrode integrated of ultrathin NiFeP on 3D strutted graphene for bifunctionally efficient overall water splitting," *Nano Energy,* vol. 58, pp. 870-876, 2019.

[43] Xiaomei Wang, W. Ma, Z. Xu, H. Wang et al., "Metal phosphide catalyst anchored on metal-caged graphitic carbon towards efficient and durable hydrogen evolution electrocatalysis," *Nano Energy,* vol. 48, pp. 500-509, 2018.

[44] Zizai Ma, R. Li, M. Wang et al., "Self-supported porous Ni-Fe-P composite as an efficient electrocatalyst for hydrofen evolution reaction in both acidic and alkaline medium," *Electrochimica Acta,* vol. 219, pp. 194-203, 2016.

[45] S. Shiva Kumar, V. Himabindu, "Hydrogen production by PEM water electrolysis – A review," *Materials Science for Energy Technologies,* vol. 2, no. 3, pp. 442-454, 2019.

[46] M. Streckova, R. Orinakova, J. Hovancova, L. Kobera, J. Brus, A.B. Hungria, V. Girman, E. Mudra, M. Heckova, M. Podobova, A. Kovalcikova, J. Dusza, "Fibrous electrocatalytic materials based on carbon/copper/copper phosphides for effective hydrogen evolution," *Applied Surface Science,* vol. 479, pp. 70-76, 2019.